Textile Research Journal

Original article

Textile Research Journal
0(00) 1–17

DOI: 10.1177/0040517518805387
journals.sagepub.com/home/trj
SAGE

Investigating the cotton ring spun yarn structure using micro computerized tomography and digital image processing techniques

Noman Haleem[1], Xin Liu[1], Christopher Hurren[1], Stuart Gordon[2], Saeed S Najar[3] and Xungai Wang[1,4]

Abstract

The micro-level structure of staple yarn and the fiber arrangement inside it has a decisive influence on its physical properties. This study aims to introduce a combined method based on micro computerized tomography (micro CT) and digital image processing techniques to probe the ring yarn structure in a non-invasive manner. Two micro CT systems at different CT settings were applied to achieve optimal quality CT images of cotton ring yarns. Three image processing algorithms were proposed to enhance and process the yarn CT images in order to extract yarn structural information. The proposed method was also applied on two yarn specimens, which varied significantly in terms of their tensile strength, to study differences in their underlying structures. The results showed that the longitudinal arrangement of fibers in terms of their migratory behavior had a decisive influence on the tensile properties of the yarn. The stronger yarn showed a higher value of the amplitude and intensity of fiber migration compared to the weaker yarn, suggesting that the protocol established in this study can effectively reveal fiber arrangements within a staple yarn structure in a non-invasive manner.

Keywords

ring yarn, yarn strength, micro computerized tomography, digital image processing

The history of research on textile yarn structure spans several decades. Initially, the yarn was thought to consist of fibers twisted in a perfectly helical arrangement around its center, but empirical evidence did not support this claim.[1,2] The tracer fiber technique revealed the occurrence of frequent radial disposition of fibers with respect to the central yarn axis (i.e. fiber migration), while the cross-sectional analysis showed non-uniform fiber packing density within a yarn.[3] In the past, both of these methods had been frequently applied on a variety of yarns to understand the fiber arrangement inside them and establish its effect on the physical characteristics (or quality) of yarns.[4–9] In addition, various developments in both of these methods were also proposed, ranging from improvements in experimental setup to automated image analysis of tracer fibers and yarn cross-sectional images.[10–15] The ultimate goal of these efforts was to improve yarn quality by understanding and manipulating the yarn structure.[16] However, both tracer fiber and microtomic analysis methods have their respective limitations.

The most critical issue related to both existing methods of yarn structural investigation is their inability to provide detailed information on yarn structure in a

[1]Deakin University, Institute for Frontier Materials, Australia
[2]CSIRO Manufacturing, Deakin University, Australia
[3]Department of Textile Engineering Department, Amirkabir University of Technology, Iran
[4]Wuhan Textile University, China

Corresponding author:
Xungai Wang, Deakin University, GTP Building, 75 Pigdons Road, Geelong, Victoria 3216, Australia.
Email: xwang@deakin.edu.au

non-invasive manner. For example, the tracer fiber method reveals the trajectory of only one (or few) fibers from a stack of tens to hundreds of fibers (depending on yarn linear density). Similarly, cross-sectional microtomy gives a snapshot only at a certain section of the yarn. In addition, both of these methods are destructive in nature and cannot be applied together on a single yarn specimen. Hence, both cross-sectional and longitudinal arrangements of fibers cannot be analyzed simultaneously. It is important to note that the complete yarn structure can only be represented by taking the cross-sectional as well as the longitudinal arrangement of fibers into account. Due to incomplete information about the internal yarn structure and the inability to study the fiber arrangement in the cross-sectional as well as the longitudinal directions simultaneously, a clear understanding of yarn structure has not yet been achieved. In addition, both of these methods are also quite invasive in nature. For example, cross-sectional microtomy requires significant physical contact during specimen preparation, handling, slicing and analyzing, which could easily affect the fragile fiber arrangement within a yarn and cause misleading observations.

Recently, an interesting idea to study yarn structure by applying micro computerized tomography (micro CT) has emerged.[17–20] Micro CT scanning is a non-invasive technique, where a specimen is exposed to X-rays at various angles around its circumference. The resulting projections are merged to produce a virtual model of the specimen, which is then sliced in the cross-sectional direction. Micro CT scanning of yarns results in a series of yarn cross-sectional images taken at fine distances (i.e. a few microns) along its length, which reveal its internal structure. Each individual CT image shows the fiber arrangement within the yarn cross-section, while stacking these CT images together reveals the longitudinal arrangement of fibers. Hence, micro CT scanning overcomes both critical limitations associated with the tracer fiber and microtomy methods in a single technique. However, prior to the application of the micro CT method to studying the yarn structure and establishing its relationships with yarn quality, two important issues need to be addressed. Firstly, micro CT scanning covers a very short yarn length (i.e. a few millimeters) due to the high-resolution scan setting, which does not provide enough information about the longitudinal arrangement of the fibers. The high resolution (around 1–2 microns) is required to view individual fibers in the CT images. Secondly, the CT images only visualize the fiber arrangement within a yarn and do not represent it in terms of suitable quantitative parameters, such as fiber migration intensity or fiber packing density.

Hence, this study aims to develop an effective method to comprehensively study yarn structure by addressing both issues associated with micro CT and applying it to investigate yarn structure–property relationships. Firstly, a yarn specimen was scanned using two different micro CT systems at variable settings to achieve an optimal quality CT image along with an acceptable length of the yarn specimen. Secondly, three image processing algorithms were developed to process the acquired yarn CT data in order to extract yarn structural information and to translate it in terms of suitable parameters. Finally, a comparison was made between the structures of two yarn specimens, which significantly differed in terms of their tensile strength, to investigate the effects of fiber arrangement within a yarn on its physical properties.

Materials and methods

Yarn specimen preparation for CT scanning

Two cotton yarn specimens of 12 tex linear density and significantly different tensile strength were selected from an experimental matrix, where yarns were produced by introducing controlled variations in the spinning triangle geometry.[21] The critical influence of spinning triangle geometry on yarn properties was established in previous studies.[22–24] The weaker and the stronger yarns had 12.9 and 16.6 cN/tex tensile strength, respectively, and were denoted as yarns L and H, respectively. Both yarns were produced from 100% Australian cotton (upper half mean length 31.5 mm, 4.5 micronaire, 84.1% length uniformity index, 7.2% short fiber index) on an industrial-scale Zinser 350 ring frame (Saurer, Switzerland). Yarn H was spun with 1108 TPM twist, high compacting pressure and a left offset diagonal spinning arrangement, while yarn L was produced with 1032 TPM twist and low compact pressure in a regular spinning arrangement (no offsetting).

Yarn H was used as the primary specimen to conduct CT optimization trials, while yarn L was only scanned at the optimal CT settings achieved for yarn H in order to compare their internal structures. As both yarn H and yarn L were produced from the same raw material and had the same linear density, the CT parameters optimized for one of them were applicable for scanning the other.

The micro CT scanning of yarn specimens required careful sample preparation. Firstly, the specimen should be mounted and kept under appropriate pretension during the whole length of the scan to avoid any unwanted movements. Secondly, the specimen should be aligned in a vertical arrangement to allow effective transmission of the X-ray beam. Hence, two tubes made up of carbon fiber and plastic material with an internal diameter of 3 mm were used as yarn sample

holders, as shown in Figure 1. The selection of either carbon fiber or plastic tube was made on the basis of X-ray beam energy selected for a particular CT trial to achieve a suitable contrast between the fibers and the background in the CT images.

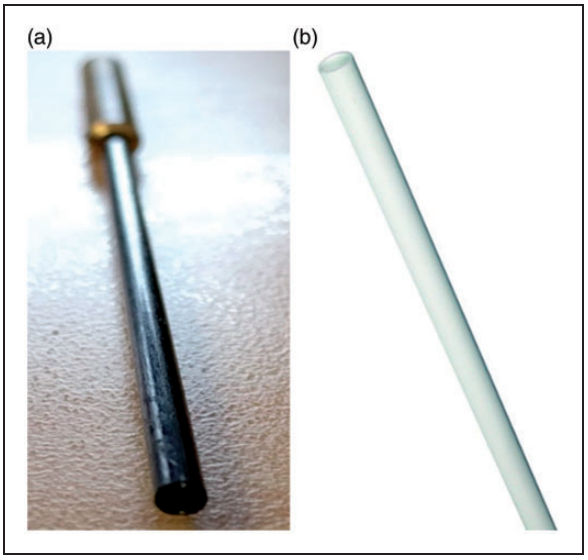

Figure 1. Specimen mounting tubes made up of (a) carbon fiber and (b) plastic material employed for micro computerized tomography experiments.

During the mounting process, one end of the specimen was taken from the yarn bobbin and was carefully threaded through the sample holder tube to avoid any loss of twist in the fibers. Some length of the yarn was also skipped to avoid scanning any yarn segment that could be interfered with during the mounting process. After threading, both ends of the yarn were taped around the outlets of the tube under pretension to keep it straight and stationary without any visible slacking. The tube was vertically mounted and tightened in the holder of the CT scanning stage in alignment with the field of view of the CT system before initiating the scanning process.

Micro CT scanning

Yarn H was scanned on two different micro CT scanners, that is, ANU Heliscan (Australian National University, Australia) and Xradia 520 Versa (Carl Zeiss GmbH, Germany), which were helical and regular type scanners, respectively. A helical type CT scanner rotates as well as vertically traverses the specimen during the scan, providing 'longer' field of view compared to a regular type CT scanner, which only rotates the specimen, as illustrated in Figure 2.

Two trials of micro CT scanning of yarns were conducted at each CT scanner and their technical

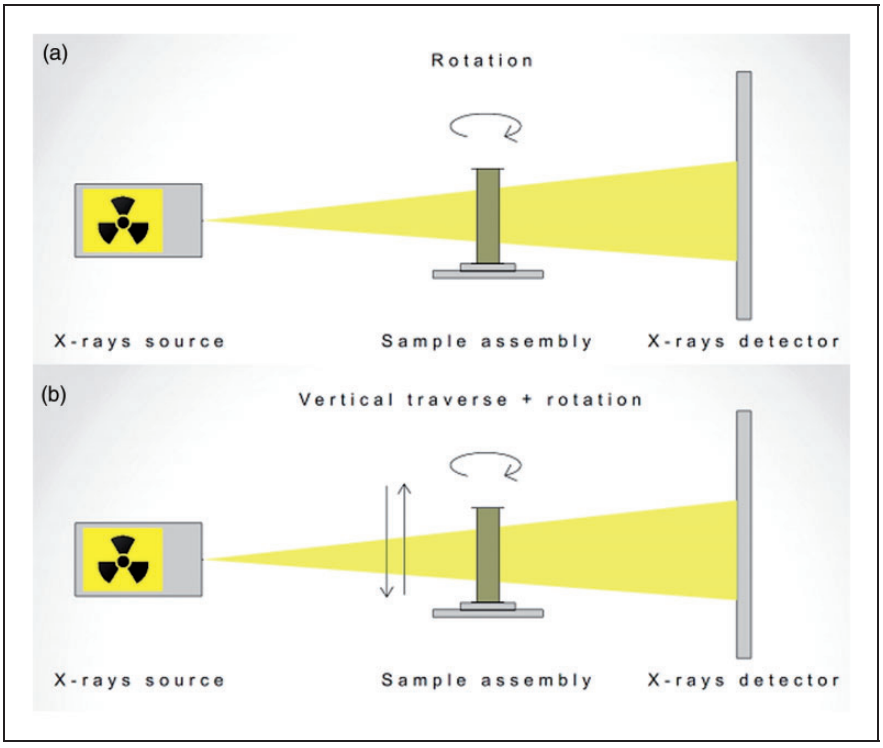

Figure 2. Two different micro computerized tomography (micro CT) scanning techniques: (a) regular micro CT scanning; (b) helical micro CT scanning.

Table 1. Detailed specifications of the yarn micro computerized tomography (micro CT) scanning trials

Parameter/scanning trial	a	b	c	d
CT scanner	Xradia 520 versa	Xradia 520 versa	ANU Heliscan micro CT	ANU Heliscan micro CT
Scanner type	Regular CT	Regular CT	Helical CT	Helical CT
Contrast technique	Absorption contrast	Absorption contrast	Absorption contrast	Absorption contrast
Sample holder type	Plastic tube	Plastic tube	Carbon fiber tube	Carbon fiber tube
Resolution/voxel (microns)	1.89	0.69	1.7	1.33
Magnification level (×)	10	40	10	110
X-ray energy (KeV)	80	80	60	60
Scan time (minutes)	30	45	680	803

specifications are given in Table 1. The parameters that were varied during CT scanning trials included the scanning resolution and the magnification, as both of them not only affected the quality and level of detail in the CT images but also affected the field of view of the CT system that is proportional to the length of the yarn covered during the scan. The scanning resolution was varied from 1.89 to 0.69 microns, while magnification was changed from 10 × to 110×. The X-ray energy was selected accordingly to achieve the desired contrast between the cotton fibers and the background in the CT images. The experimental arrangement for micro CT scanning for the helical type CT scanner is shown in Figure 3.

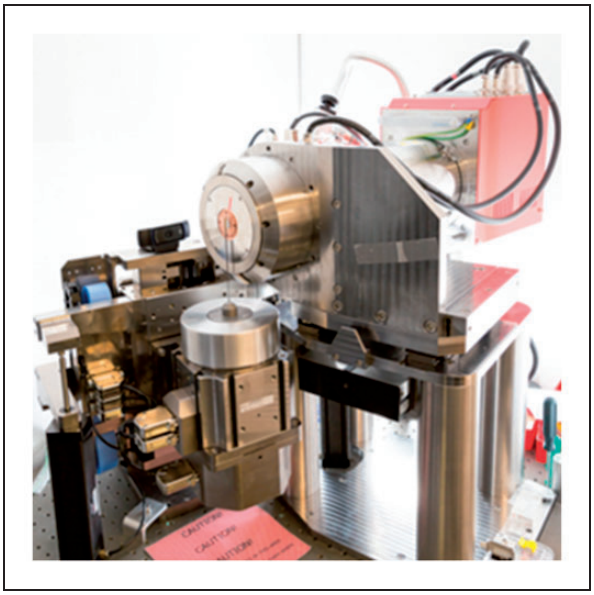

Figure 3. Experimental arrangement of the helical type micro computerized tomography scanner.

Image processing

The optimal quality CT datasets of yarns H and L that were achieved through the above-mentioned trials were selected for processing and extracting the yarn structure-related information. The complete datasets contained 306 discreet blocks in Network Common Data Form (NetCDF) file format and each block consisted of 40 images, which resulted in a total of 12,240 serial CT images. These images were first extracted from the blocks and then converted into TIF file format. The CT datasets were processed through three different image processing algorithms that were developed in MATLAB R2016a (MathWorks, USA) by using various functions from the image processing, signal processing and statistical toolboxes. The proposed algorithms enhanced the CT images, analyzed fiber arrangement in the yarn cross-section and tracked fiber paths along the yarn length. The algorithms processed the CT dataset in an automated manner to avoid the laborious and time consuming task of manual processing. ImageJ 1.46r (National Institutes of Health, USA) with the three-dimensional (3D) viewer plugin was used for visualizing the datasets. A high-performance computing cluster called the Multi-modal Australian ScienceS Imaging and Visualization Environment (MASSIVE) was used for processing the CT images by the developed algorithms. The details of the image processing work flow of all three algorithms are given as follows.

Algorithm for image enhancement

The yarn CT dataset intrinsically contained artifacts and unwanted features such as random noise and an uneven background. In order to apply the image processing operations and to quantify the information of interest out of the CT images, some degree of pre-processing or enhancement was essential. The first image processing algorithm focused on image enhancement and it worked in the following sequence:

reading every single image (one at a time) from the CT dataset into MATLAB workspace;

increasing the image size by a factor of two using 'bicubic' interpolation to improve its digital resolution;
smoothing the image using a 'Gaussian filter' at sigma level 0.5 to minimize the normally distributed noise;
improving the image contrast by mapping the pixels with grayscale intensity values between 0.4 and 0.6 such that 1% data (or pixels) was saturated at the lowest and highest intensity values;
taking the first-order derivative of the pixels intensities in the spatial domain along the x-axis, y-axis, + 45° and –45° directions, using the following mathematical relation

$$\frac{\partial f}{\partial x} = f(x+1) - f(x) \tag{1}$$

where $\frac{\partial f}{\partial x}$ is the derivative of pixels x and $x+1$, which lie along the x-axis, $f(x)$ is the grayscale intensity value of pixel x and $f(x+1)$ is the grayscale intensity value of pixel $x+1$;
imposing the fiber boundaries achieved through the derivative operation on the original CT image to suppress its background;
taking the second derivative of the resultant image along the x-axis, y-axis, + 45° and –45° directions, according to the following relation

$$\frac{\partial^2 f}{\partial x^2} = f(x+1) + f(x-1) - 2f(x) \tag{2}$$

where $\frac{\partial^2 f}{\partial x^2}$ is the second derivative of the pixel $f(x)$, $f(x)$ is the grayscale value of pixel x, $f(x+1)$ is the grayscale value of pixel $x+1$, lying next to pixel x and $f(x-1)$ is the grayscale value of pixel x–1, lying before pixel x;
subtracting the second derivative image from the image achieved in step 6 to eliminate noise pixels/objects from the background;
converting the segmented image to a binary image (at 0.1 threshold value) using Otsu's method;[25]
imposing the binary image onto the original CT image such that the pixels having a value of 1 in the binary image remain unchanged, while the pixels having a value of 0 in the binary image are set to 0;
filling the small holes within the fibers through the image flood filling operation;
eliminating any isolated objects in the image less than an area of 20 pixels, which represented random noise pixels/objects arising from unwanted artifacts in the CT image.

Algorithm for yarn cross-sectional analysis

The information related to fiber arrangement in the yarn structure was spread along two dimensions of the CT dataset, that is, within the yarn cross-section and along the yarn length. The second image processing algorithm dealt with analyzing the pre-processed CT images (achieved from the first algorithm) and quantifying the yarn structural parameters related to the cross-sectional arrangement of fibers. The sequence of image processing operations involved in the second algorithm is given as follows:

reading the binary version of the pre-processed yarn CT image (as achieved from the first algorithm) into MATLAB workspace;

dilating the image with a disk shape structuring element (radius 3 pixels) to increase the fiber diameters to merge them together into a single object;

keeping only the largest object (connected fibrous cluster) in the CT image through the size threshold and eliminating other objects that represented distant fibers, that is, hairs;

determining the center of the connected fibrous cluster (i.e. center of mass as calculated by linear weighing of the pixels) and taking it as the yarn center;

marking the yarn center on the image in step 1 and eliminating the hair fibers by Euclidean distance threshold by measurement of the yarn radius based on its count (i.e. fineness), as given in Equation (3)[26]

$$Y_{rad} = \frac{1}{56\sqrt{Ne}} \tag{3}$$

applying morphological dilation followed by morphological erosion through a disk shape structuring element (radius 15 pixels) on the remaining fibers to determine the yarn boundary;

calculating the total number of white pixels inside the yarn boundary, which represent the total fiber area within the yarn cross-section;

calculating the total number of pixels within the yarn boundary, which represent the total yarn area.

The determination of the yarn boundary and the measurement of total yarn and fiber areas led to the calculation of some established parameters that represented the yarn structure, such as the fiber packing density, yarn diameter, yarn radial packing density, yarn shape factor and the number of fibers in the yarn cross-section.

Algorithm for yarn longitudinal analysis

The third image processing algorithm analyzed the longitudinal arrangement of fibers along the yarn length. It involved motion-based segmentation and region growing techniques to first segment the connected fibers into individual objects followed by tracking their movement through each individual CT image in the dataset. The spatial coordinates of the centroid of each fiber were

recorded to later draw and analyze their trajectories. The various steps involved in the third image processing algorithm are sequenced as follows.

Manually segmenting the individual fibers in the first image (N) of the CT dataset, reading it into MATLAB workspace and labeling each individual fiber inside it with a number in incremental order, that is, 1, 2, 3, ..., All other pixels that did not belong to any fiber in N were assigned a value of 0.

Reading the second pre-processed CT image ($N + 1$) into MATLAB workspace.

Converting image $N + 1$ into a binary image with threshold value 0, which means all pixels with a value greater than 0 in $N + 1$ will be assigned 1 in the respective binary image.

Labeling each object (either a single fiber or a cluster of fibers) in the binary image $N + 1$ and recording the coordinates of each pixel that belong to each object.

Taking a Boolean image intersection of each fiber lying in the image N with each individual object in image $N + 1$.

All pixels of image $N + 1$ that were matched with a particular object (or fiber) in image N were assigned the same number as that of the matching object in N, leading to segmentation of individual fibers. The remaining pixels of $N + 1$ were assigned a 0 value.

The area (or number of pixels) of each segmented fiber in image $N + 1$ was grown in 20 iterations under that condition that it would not exceed the area of the fiber in image N.

A similar operation was then repeated on image $N + 2$ by taking image $N + 1$ as a reference image, which was already segmented and the loop continued on all images throughout the length of the CT dataset.

Results and discussion

Optimization of micro CT scanning for yarn specimen

The CT images of cotton yarn specimens acquired through four different trials of micro CT scanning are shown in Figure 4 and labeled with the respective trial IDs as assigned in Table 1. Trials (a) and (b) were conducted on a regular type, while trials (c) and (d) were conducted on a helical type micro CT system. In the CT trial (a), which was both a low-resolution (1.89 microns) and low-magnification (10×) CT experiment,

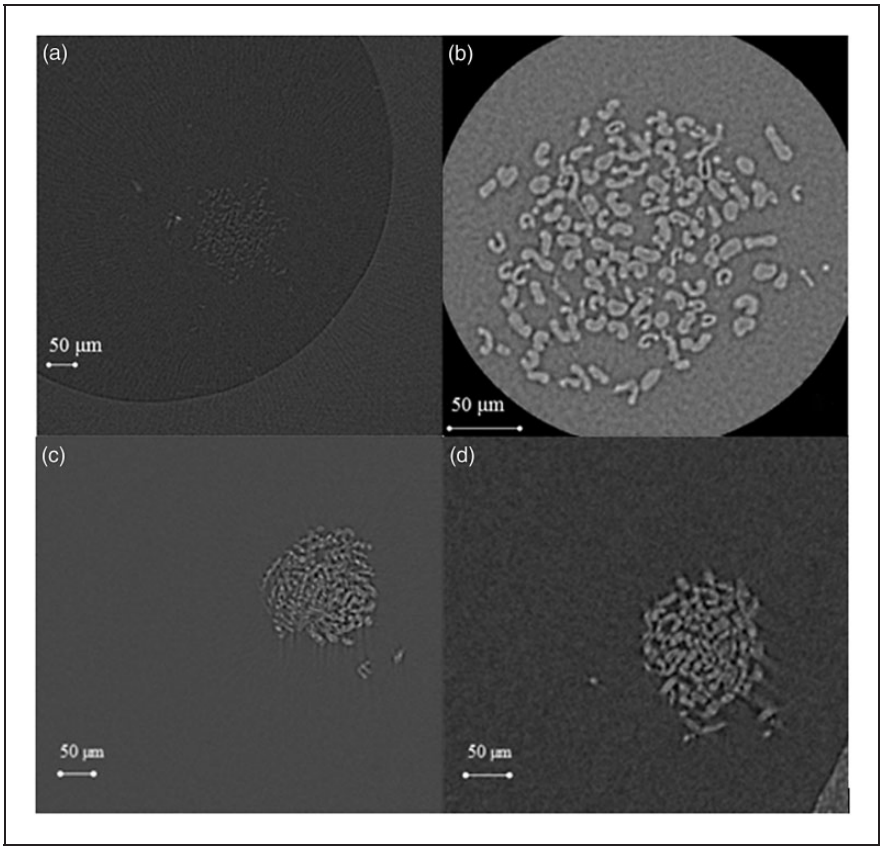

Figure 4. Micro computerized tomography scanning of yarns with (a) and (b), regular type, and (c) and (d), helical type scanners.

1.88 millimeter yarn length was scanned, and one of the resultant CT images is shown in Figure 4(a). The individual fibers inside the yarn can be seen as small light colored dots against the darker background. However, a clear view of the individual fibers is not achieved, as the boundaries of the individual fibers are not visually separable from each other. The low scanning resolution and magnification together resulted in poor optical resolution of the CT system that was not substantial enough to effectively resolve the fine fiber dimensions and even finer inter fiber spacing in the resultant yarn CT image. The CT image achieved through trial (a) did not carry enough and clear enough information about the yarn structure and cannot be processed further to analyze the fiber arrangement within the yarn.

The first CT trial clearly indicates the essential need of increasing the scanning resolution and the magnification to improve the visualization of the individual cotton fibers. Hence, trial (b) was conducted at 0.69 micron resolution and $40\times$ magnification, and the resultant CT image is shown in Figure 4(b). The increment in scanning resolution and magnification has clearly improved the quality and the level of detail, as the individual fibers can now be clearly seen in the CT image. In addition, the cross-sectional profile and perimeter of each fiber are also evident. The peripheries of the fibers in the CT image are slightly darker (low intensity value) than the rest of the fiber, producing a superior contrast between the fibers and the background, making it very suitable for downstream image processing and yarn structural analysis. However, the major issue associated with trial (b) is very limited yarn length (i.e. 0.35 millimeter or 350 microns), as high resolution and magnification settings narrow down the field of view of the CT system. Such a short yarn length does not provide enough information about the longitudinal arrangement of fibers within the yarn, which is essential to build a comprehensive understanding of the yarn structure.

One possibility to resolve this problem is serial CT scanning, where multiple regular scans are conducted on a single specimen at various segments and the resultant CT volumes are stitched together to achieve a larger field of view without compromising on the scanning resolution. However, the requirement of yarn length in this case is around 30 mm (i.e. the approximate length of a single cotton fiber) to allow tracking the longitudinal arrangement of fibers inside the yarn. In order to achieve this length at 0.69 micron scanning resolution on a regular type CT system, at least 86 serial scans are required. The number of serial scans could even increase, as the stitching process requires some overlapping length of the volumes, making the whole process very intensive in terms of cost, resources and time. Another possibility is to use a helical type CT scanning system, which scans the specimen in a helical trajectory arrangement, which covers a longer specimen length without the need to stitch multiple volumes together. Helical CT scanning is also a time consuming and resource intensive process, but the associated costs are substantially less than those for the serial scanning method on a regular type CT system.

The CT trial (c) was conducted on a helical type micro CT scanner at 1.7 micron scanning resolution and $10\times$ magnification. The scan covered 19.4 mm yarn length, and the resultant CT image is shown in Figure 4(c). The view of the fibers in the CT image is superior to what was achieved in trial (a), as individual fibers can be separately noticed to some extent. However, the CT image is not as superior as the one achieved in CT trial (b). The optical resolution of the CT system was not substantial enough to effectively visualize fine inter fiber spacing due to limited scanning resolution, and further image analysis could not be performed to analyze the yarn structure. Hence, the scanning resolution must be increased to improve the level of detail in the CT image. However, the impressive feature of trial (c) is that it covered a 19.4 mm yarn length in a single scan. This length is around 10 times longer than the yarn length achieved in trial (a) and 55 times longer than the yarn length achieved in trial (b). This shows that helical CT scanning is more suitable for scanning specimens with a higher aspect ratio, such as textile yarns, compared to regular CT scanning.

The last CT trial (d) was also conducted on a helical type CT system at 1.33 micron scanning resolution and $110\times$ magnification. The scan covered a 16.28 mm yarn length, and the resultant CT image is shown in Figure 4(d). The CT image achieved through trial (d) is superior in quality and level of detail to the CT image achieved through trial (c). The fibers have an improved contrast against the background. The inter fiber spacing is not as clearly visible as it was in case of CT trial (b) on a regular CT system, but the darker edges of the fibers makes them visually separable from each other. Although the quality of the CT image can be further improved by increasing the scanning resolution, it would be a compromise on the yarn length scanned (i.e. 16.28 mm), which is highly undesired. Although 16.28 mm does not represent the average (upper half mean) length of a cotton fiber, it can still provide some useful insight into the longitudinal arrangement of fibers. The yarn length covered in CT trial (d) was slightly less than the yarn length achieved in CT trial (c), but it is still much higher than the yarn length achieved in trials (a) and (b). Hence, in assessing the outcomes achieved through the four different CT trials, the CT settings for trial (d) using a helical type CT system were selected as optimal for scanning yarn specimens. Two typical CT images of yarns

H and L acquired through these trials are shown in Figures 5(a) and (b).

Analyzing yarn structure using digital image processing

The CT image datasets of both yarns L and H were processed using three image processing algorithms in order to extract yarn structural information and express it in terms of suitable parameters. The application of image processing algorithms on a CT image sequence to quantify the yarn structure is presented and discussed as follows.

Image enhancement. It can be clearly seen that the CT image in its original form cannot be used for image analysis due to the presence of unwanted features, such as random noise and an inconsistent background, which surrounds the cotton fibers and blurs their boundaries and perimeters to some extent. These undesired features shadow the information of interest in the CT images and would not allow direct application of image processing operations to segment individual fibers and analyze their arrangement. Hence, the first image processing algorithm focused on enhancing the yarn CT images by improving their appearance and eliminating unwanted features from them.

The outcomes of various steps involved in the image enhancement process are given in Figure 6, where Figure 6(a) shows the original CT image, which was resized by a factor of 2 to improve its digital resolution. Figures 6(b) and (c) show the outcomes of Gaussian filtering to minimize normally distributed noise in the image followed by image contrast adjustment, respectively. Although contrast adjustment segmented most of the fibrous regions from the background, due to non-uniformity within the fibrous regions as well as in the background an effective segmentation was not achieved, which could affect downstream image processing. To counter this issue, the first-order derivative operation was applied, and the resultant image is shown in Figure 6(d). The first-order derivative results in higher values at steeper intensity gradients (which occur at the fiber boundary) compared to gradual intensity gradients (which occur within the fiber region).[27] The fiber boundaries as determined by derivative operations were then imposed on the image shown in Figure 6(c) to emphasize the fibrous areas and suppress the background, as shown in Figure 6(e). Although the fiber segmentation was slightly improved by the derivative operation, some small white objects can still be observed in the background that do not belong to any fiber and should be removed. Hence, the second-order derivative operation was applied as it has an aggressive response (as it assigns high pixel values) to the finer details in the image (such as thin lines and isolated points) compared to the first-order derivative operation. The application of the second derivative is shown in Figure 6(f), which was then subtracted from the image in Figure 6(e) to achieve a uniform background, as shown in Figure 6(g).

The binary conversion was applied on the second derivative image, as shown in Figure 6(h), and the resultant binary mask was imposed on the Gaussian noise removed image, that is, Figure 6(b), to segment the fiber regions, as shown in Figure 6(i). In order to compensate for the small holes within the fibers at low intensity areas, the flood filling morphological operation was applied and its outcome is shown in Figure 6(j). Several small-sized objects that could still

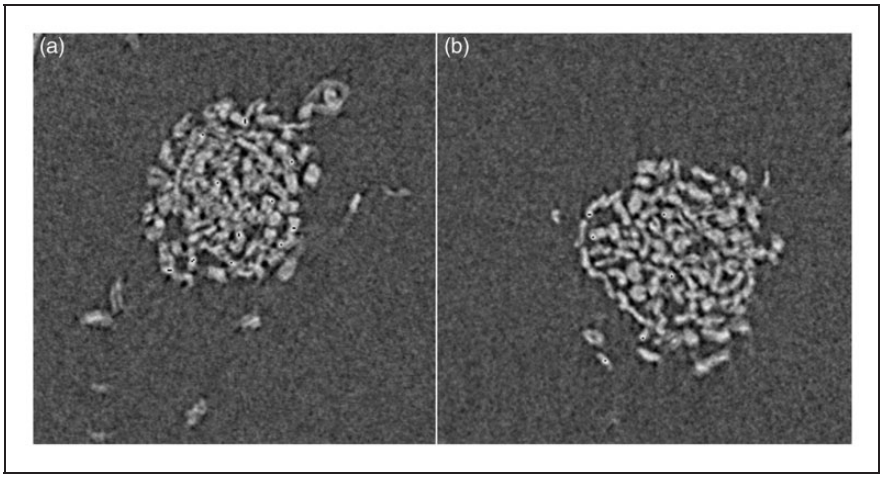

Figure 5. Micro computerized tomography (micro CT) images of (a) yarn H and (b) yarn L from respective CT datasets.

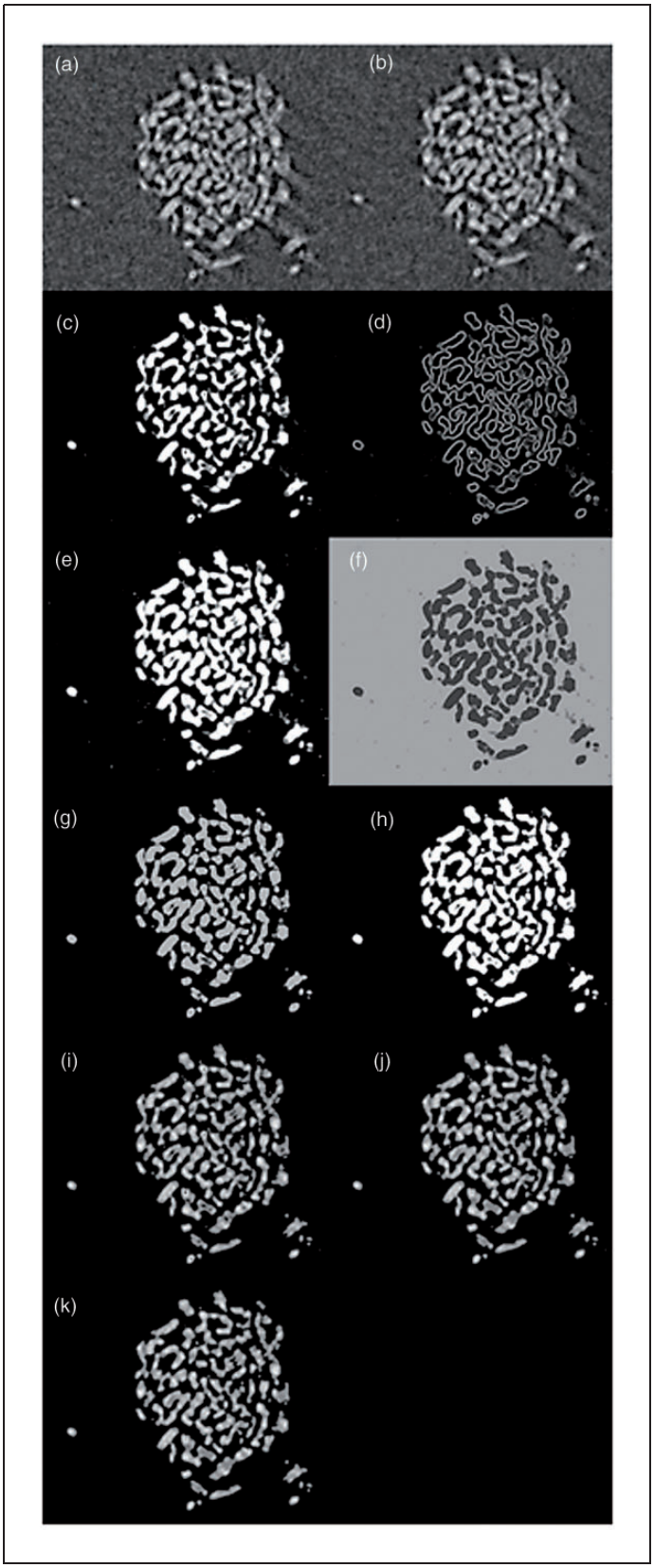

Figure 6. Various stages involved in the image enhancement algorithm (a) original computerized tomography image; (b) Gaussian filtering; (c) contrast adjustment; (d) first derivative of the image achieved in step (c); (e) image (d) imposed on image (c); (f) second-order derivative of image (e); (g) subtracting image (f) from image (e); (h) binary conversion of image (g); (i) imposing image (h) on image (b); (j) flood filling operation applied on image (i); (k) size threshold for objects more than 20 pixels in size

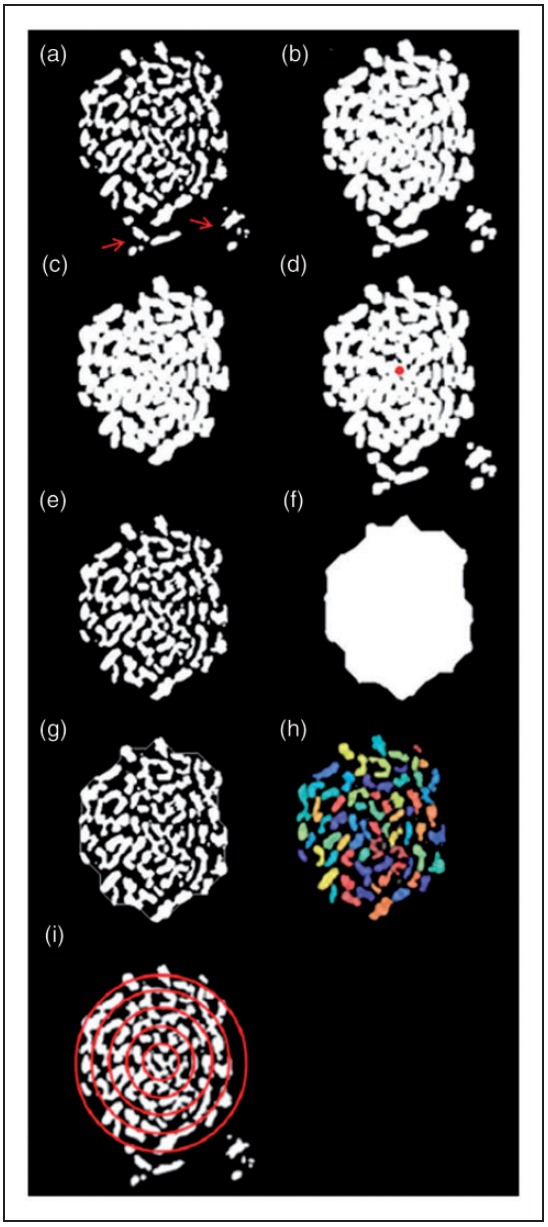

Figure 7. Various stages in the calculation of different yarn structural parameters related to the cross-sectional distribution of fibers: a) binary version of the enhanced micro computerized tomography image with hair fibers highlighted; (b) morphological dilation; (c) area thresholding to isolate hair fibers; (d) determination of the yarn center; (e) hair elimination by distance thresholding; (f) morphological dilation followed by morphological erosion; (g) yarn boundary tracing; (h) individual segmented fibers within the yarn cross-section; (i) measurement of yarn radial packing density by dividing the cross-section into concentric circular zones. (Color online only.)

be noticed around the fibers were removed through the size threshold operation by removing any objects less than 20 pixels in size. The final form of the enhanced image is shown in Figure 6(k).

Analysis of fiber arrangement in the yarn cross-section

The minimization of noise and subtraction of the inconsistent background in the yarn CT image allowed image analysis to quantify yarn structure-related information, which lies in two different dimensions of the CT dataset, that is, within the yarn cross-section and along the yarn length. The second image processing algorithm analyzes the fiber arrangement within the yarn cross-section and reports it in terms of fiber packing density, equivalent diameter of yarn, number of fibers in yarn cross-section, fiber radial packing density and yarn shape factor. The outcomes of the application of the second image processing algorithm in terms of images at various steps of its workflow are shown in Figure 7. The first requirement of the cross-sectional analysis is the identification of hair fibers from the CT image. The hairs are those fibers that lie at some distance from the main yarn body. Hair fibers not only lie at the highest Euclidean distance from the yarn center, but also lie far apart from their neighboring fibers. Some hair fibers are indicated with red arrows in the lower right corner and at the bottom center of Figure 7(a), which is the binary form of the previously enhanced image. Prior to measurement of any cross-section-related parameters, the main yarn body should be segmented from the hair fibers.

In order to identify and remove hair fibers, morphological dilation was carried out on the binary image with a disk-shaped structuring element (3 pixel radius), as shown in Figure 7(b), to achieve two purposes. Firstly, those fibers that belong to the main yarn body and essentially lie close to their neighboring fibers would eventually touch and merge into each other to form a single large fibrous cluster (or object). The hairs, which lie at a distance from their neighboring fibers, would not become a part of this fibrous cluster and could simply be eliminated by object size thresholding, as shown in Figure 7(c). Secondly, the yarn center can be determined simply by linearly averaging the spatial coordinates (both x and y) of all pixels that belong to the fiber mass shown in Figure 7(c). The yarn center is then represented with a red dot in Figure 7(d). The final step of eliminating hair fibers was to measure the distance of each fiber in Figure 7(a) from the nominated yarn center and, if it exceeded the yarn radius threshold (as calculated by Equation (3)), the fiber was considered a hair and eliminated, as shown in Figure 7(e). These dual criteria for the detection and removal of hairs ensured accuracy and avoided unnecessary removal of fibers, which could significantly influence the value of the calculated parameters. The total fiber area was then simply calculated as the total number of white pixels in the image.

After isolating hair fibers, the next step was to nominate the yarn boundary to allow calculation of the total yarn area. This was achieved by morphological dilation followed by morphological erosion of the image shown in Figure 7(e) with a disk-shaped structuring element (radius 15 pixels), and the resultant image is shown in Figure 7(f). The dilation operation increased the size of each fiber to the extent that all fibers merged into each other to form a single object. The successive erosion of that object removed added pixels from its edges, bringing its size back to normal. The boundary of the eroded fibrous object represented the yarn boundary as it is imposed on the initial CT image, and is shown in Figure 7(g). The total number of pixels within the yarn boundary (including boundary pixels) represented the total yarn area.

The measurement of total fiber and yarn areas led to the calculation of fiber packing density, which is defined as the ratio of the former to the latter.[12] The radial packing density of a yarn, which represents fiber packing as a function of yarn radius, was calculated by dividing the yarn cross-section into five concentric circular regions at equal radial distance from the yarn center, as shown in Figure 7(i).[3] All five circles with radii of 25, 50, 75, 100 and 125 microns are centered at the yarn center. The packing density in each circular region was calculated as the ratio of total white pixels (i.e. fiber area) to the total number of pixels inside it. In order to calculate the total number of fibers in the yarn cross-section, individual fiber segmentation was achieved through the third image processing algorithm (whose details are given in the next section), as shown in Figure 7(h).

The yarn diameter was calculated as the equivalent diameter because the yarn cross-section was an arbitrary shape instead of a perfect circle, as is generally assumed. The equivalent yarn diameter was the diameter of an imaginary circle with an area exactly equal to the total area of the yarn, and was calculated using Equation (4).[28] The yarn diameter value was also divided by a factor of 2 to compensate for image resizing (where the image size was enhanced by a factor of 2, as described in the image enhancement algorithm). The yarn shape factor is a new parameter to characterize the degree of circularity of the yarn cross-sectional profile; its value ranges from 0 to 1, where 0 indicates an ideal circle and 1 refers to a straight line. However, both 0 and 1 are extreme cases. A higher value of the shape factor refers to an irregular arrangement of fibers, while its lower value refers to fiber arrangement in a perfectly circular arrangement. The yarn shape factor was calculated from Equation (5) by assuming the yarn cross-sectional shape as an ellipse and taking the ratio of its smallest and largest diameters.[29] The above-mentioned parameters were measured in pixel units (except unitless quantities), which were then converted into physical units (i.e. microns) simply by multiplying them by the scanning voxel size, that is, 1.33 microns

$$YD_{EQ} = \sqrt{\frac{4 \times Py}{\pi}} \tag{4}$$

where YD_{EQ} is the equivalent diameter of the yarn and P_y is the total number of pixels lying within the yarn boundary (i.e. the yarn area)

$$YS = \frac{L_f}{L_{ma}} \tag{5}$$

where YS is the yarn shape factor, L_f is the distance between the foci of the ellipse of the yarn cross-section and L_{ma} is the length of the major axis of the ellipse of the yarn cross-section.

Analysis of fiber arrangement along the yarn length

In order to analyze the longitudinal arrangement of fibers within a yarn, tracking of the fiber path along the yarn length is essential, which requires the accurate segmentation of individual fibers in each image throughout the CT dataset. The fibers in the CT image appear to be 'connected' with each other in the form of small clusters and could not be segmented based on their physical characteristics (i.e. grayscale intensity, size or shape) due to significant variations in them both within the CT image and across the CT dataset. However, one possibility to segment individual fibers is through motion-based segmentation by tracking slight changes in fiber positions between two consecutive CT images. The physical distance between two consecutive CT slices was 1.33 microns (i.e. the scanning voxel size) and changes in fiber positions were very small, as could be noticed in four consecutive CT images (i.e. N, $N+1$, $N+2$ and $N+3$) in Figures 8(a)–(d). In order to provide a reference to initiate motion-based segmentation, the first image in the series, that is, N, was manually segmented, as shown in Figure 8(e). The reference image N was converted to a binary image and all individual fibers were labeled and assigned a distinct number and red, green, blue (RGB) value. Each object (i.e. fiber) in image N was then compared with all objects (or fibers) present in image $N+1$. The overlapping regions of the matching objects in $N+1$ were assigned the number and RGB value of the respective object in image N, as shown in Figures 8(e) and (f).

Similarly, in the following images of the series, the fiber segmentation was carried out in consecutive pair form (i.e. $N+1$ and $N+2$, $N+2$ and $N+3$ and so on). The first part of the pair was a reference image,

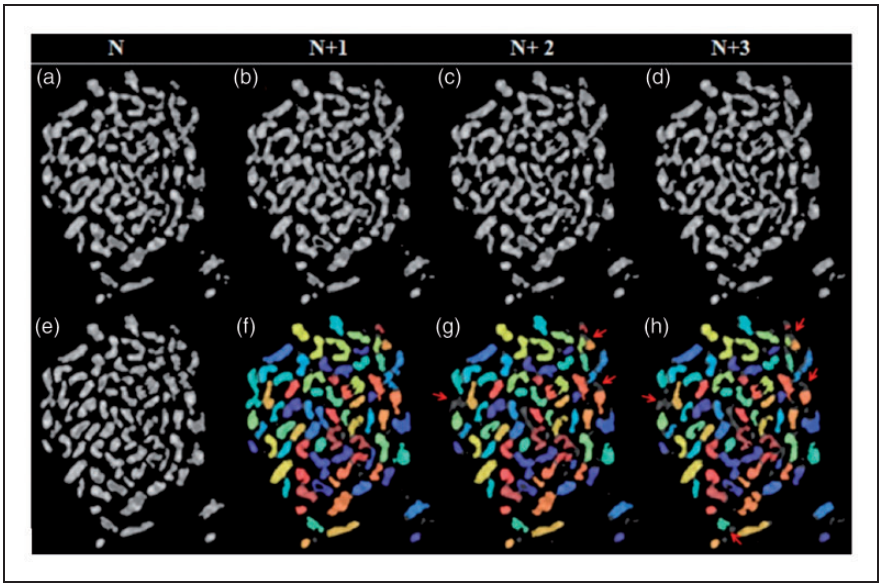

Figure 8. Motion-based segmentation to track individual fibers in yarn computerized tomography images. (Color online only.)

while the second part was the image to be segmented. The outcomes of the following image segmentation are shown in Figures 8(g) and (h). However, one problem associated with motion-based segmentation is shrinkage in the overlapping fiber areas as the segmentation operation proceeds along yarn length. This can be noticed in Figures 8(g) and (h), which shows small grayish regions (indicated by small red arrows) that do not overlap with any object in their preceding image. If the grayish areas keep on increasing with each image, eventually the track of the fibers being traced will be lost, which must be avoided in order to extract the longitudinal arrangement of fibers within the yarn.

In order to address this issue, region growth techniques were used to grow the area of fibers in the grayish zones in each CT image. The regions were grown in several iterations by comparing the total area of each fiber (motion segmented area and grown area) in a CT image with the area of the respective fiber in the previous CT image. The grown regions for images N, $N + 1$ and $N + 2$ are shown in Figures 9(a)–(c), respectively. The final outcomes of individual fiber tracking by combining motion-based segmentation with the region growing technique are shown in Figures 9(d)–(g), where the gray areas were assigned the RGB values of the respective fibers, as shown with small green arrows.

The final processed CT images were stacked together to visualize their longitudinal arrangement inside the yarn, as shown in Figure 10, where each fiber has been illustrated in a different color according to the RGB value assigned to it during tracking. The volume shown in Figure 10 consisted of 500 processed CT images. The spatial coordinates of all segmented fibers were recorded to extract their 3D trajectories. The yarn structural parameters related to the longitudinal arrangement of fibers, such as mean fiber position, migration amplitude and intensity, were calculated using equations proposed by Hearle et al.[30] In addition, another parameter, that is, the migration factor, which represented the overall extent of fiber migration occurring within a yarn, was also calculated as proposed by Huh et al.[11] and given in Equation (6)

$$\begin{aligned} \textit{migration factor} = {} & (\textit{RMS deviation}) \\ & \times (\textit{migration intensity}) \end{aligned} \tag{6}$$

Comparison of yarn structures

The CT datasets of both yarns H and L were processed using the above-mentioned image processing algorithms and the yarn structure was then reported in terms of parameters that represented fiber arrangement within the yarn cross-section and along the yarn length. The parameters related to fiber arrangement within the yarn cross-section were calculated from each CT image in the dataset, resulting in a total of 12,240 observations. The value of each parameter represents the average of these observations, and the extent of variation within them is given by the standard deviation, as shown in Table 2. The parameters related to the longitudinal arrangement of fibers were calculated by tracking the spatial coordinates of each individual fiber, and their values represent an average of all fibers within the

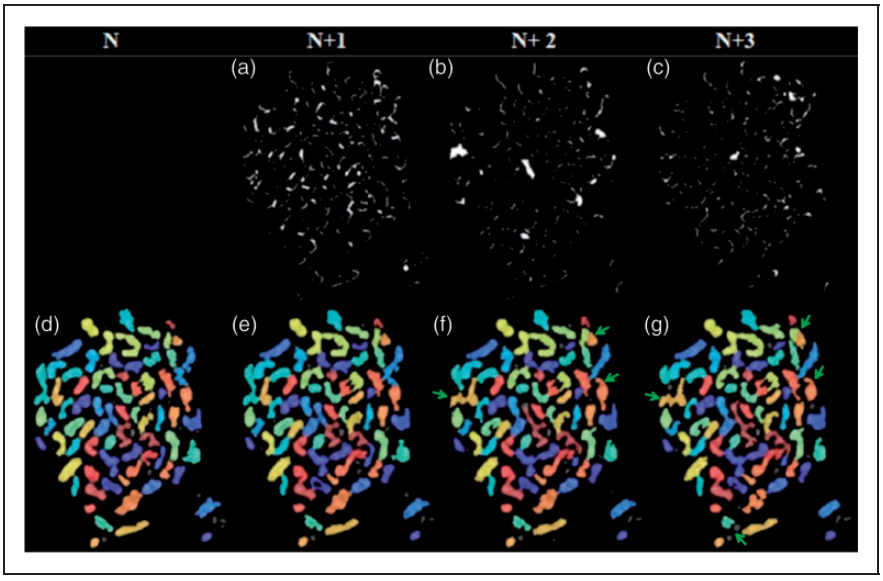

Figure 9. Application of the region growing method on motion segmented images to keep track of individual fibers. (Color online only.)

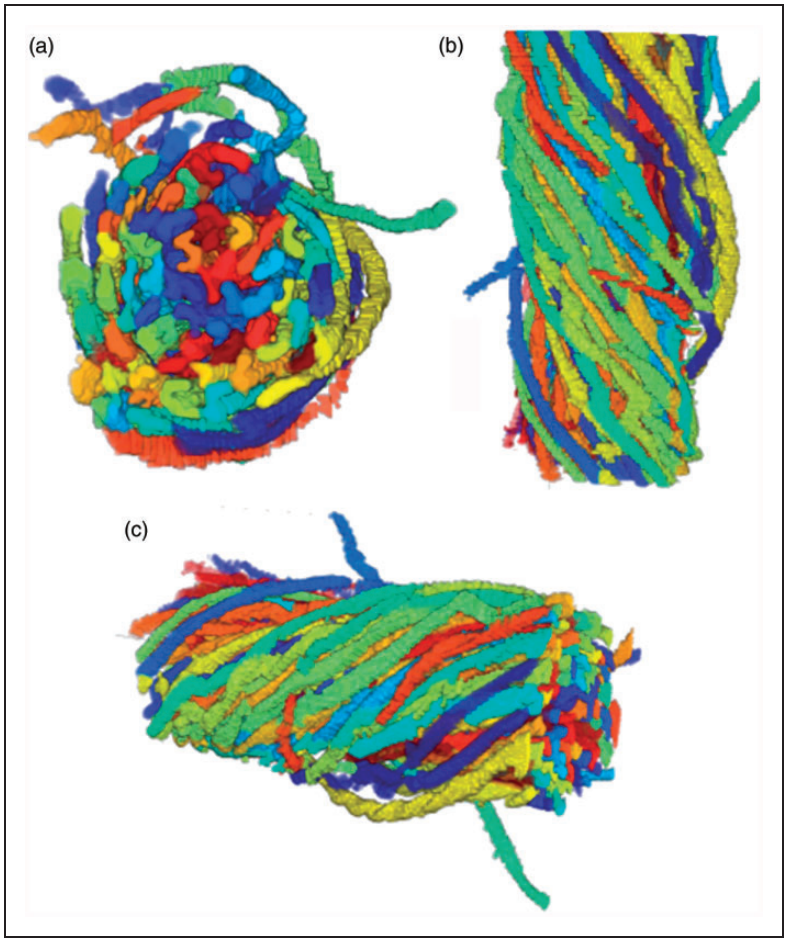

Figure 10. Different views of the three-dimensional volume of the yarn specimen achieved through vertical stacking of computerized tomography images (a) Top view, (b) Side view, (c) 3D view.

Table 2. Yarn structural parameters related to fiber distribution in the yarn cross-section

Parameters	Specimen ID	
	Yarn H	Yarn L
Equivalent diameter of yarn (μm)	153.35 ± 5.7	156.95 ± 4.15
Fiber packing density	0.499 ± 0.02	0.494 ± 0.02
Yarn shape factor	0.39 ± 0.1	0.37 ± 0.1
Average number of fibers	80 ± 8	81 ± 8
Radial packing density		
Zone A	0.51 ± 0.05	0.53 ± 0.05
Zone B	0.51 ± 0.03	0.52 ± 0.03
Zone C	0.5 ± 0.03	0.5 ± 0.03
Zone D	0.46 ± 0.03	0.46 ± 0.03
Zone E	0.29 ± 0.07	0.34 ± 0.05

Table 3. Yarn structural parameters related to fiber arrangement along the yarn length

Parameters	Specimen ID	
	Yarn H	Yarn L
Mean fiber position ($\bar{Y}$)	0.31 ± 0.4	0.21 ± 0.23
Mean amplitude of migration (A)	0.43 ± 0.35	0.36 ± 0.17
Mean migration intensity (I) (voxel^{-1} i.e. 1.33 μm)	1.61 ± 0.05	1.36 ± 0.02
Migration factor	0.23	0.16

yarn, as given in Table 3. The significance of differences between the structural parameters of yarns H and L was determined by a Student's *t*-test at the 95% confidence interval.

The comparison of the yarn structural parameters related to fiber distribution within the yarn cross-section shows only slight differences between yarns H and L. The equivalent diameter of yarn H (i.e. 153.35 microns) is slightly smaller than that of yarn L (i.e. 156.95 microns), but this minor difference is statistically significant (*P*-value = 0.001). It is worth noting the large sample sizes, that is, 12,240 observations of each parameter were made relating to each single image of the CT dataset. The diameter of 12 tex yarn calculated using the relation given in Equation (3) was 129.31 microns, which is relatively smaller than the yarn diameter calculated by the proposed image processing algorithm. However, it should be noted that the yarn diameter calculated by the image processing method is not the actual diameter but the equivalent diameter of the yarn. The yarn diameter is generally considered as a function of the total number of fibers within the yarn cross-section, which then relies on the yarn linear density.[31] As the linear density of both yarns was 12 tex, the average number of fibers within the yarn cross-section was also almost equal, that is, 80 for yarn H and 81 for yarn L. However, this is greater than the number of fibers calculated by taking the ratio of yarn and fiber linear densities (i.e. 12 and 0.177 tex, respectively), which was around 68. This difference in the number of fibers could be attributed to limited CT scanning resolution, due to which the fibers appeared to be connected in small clusters. Hence, individual fiber segmentation was not achieved effectively, which would have influenced the measurement values. Based on the limited differences between the yarn diameter and the total number of fibers within the yarn cross-section, both of these parameters can be considered non-influencing on yarn strength.

The difference between the fiber packing density of yarn H (i.e. 0.499) and yarn L (i.e. 0.494) was also minimal but statistically significant (*P*-value = 0.001). Similarly, the pattern of radial packing density of both yarns in terms of the fiber area lying in each circular zone around the yarn center was similar. The radial packing density was the highest around the yarn center and intermediate fibrous zones, as calculated in circular zones A, B and C (around 0.5). The radial packing density then slightly decreased in zone D (i.e. 0.46) and dropped quite significantly in zone E (i.e. around 0.3). The difference between the packing densities in zones A, B and E for both yarns was statistically significant (*P*-value = 0.001), while the difference between the number of fibers in zones C and D was non-significant (*P*-value = 1). This indicated that the fiber packing density in terms of area occupied by the fibers and their distribution in the radial zones around the yarn center did not greatly differ between the two yarns and most likely did not influence the yarn strength. This lack of difference between packing densities could be attributed to the fact that both of these yarns were produced through compact spinning (although at different compacting pressures).

The areal packing density and its distribution with respect to yarn radius are in close agreement with the previously reported studies, although the value of the packing density for the compact yarn presented in Table 2 appears to be on the lower side (i.e. 0499 and 0.494).[3,12,32–34] One possible explanation for this could be the compressive force exerted on fibers, as the yarn specimen is embedded and cured into a resin or wax medium during sample preparation for cross-sectional microtomy, as reported in above-mentioned studies. This could increase the packing density of fibers by pushing them closer to each other. As the micro CT method did not require a similar sample preparation, the packing density values remained on the lower side.

The comparison of the shape factors of both yarns indicated the lack of substantial difference between them, as the shape factors for yarns H and L were 0.39 and 0.37, respectively, although it was statistically significant (P-value = 0.001). The values of the shape factor indicated that none of the yarns exhibited a perfectly circular profile of their cross-section, but instead it was arbitrary.

The yarn structural parameters related to the longitudinal arrangement of fibers within the yarn describe the extent of fiber migration by representing the magnitude of variations in the radial position of a fiber with respect to the yarn central axis. The mean fiber positions calculated for yarns H and L were 0.31 and 0.21, respectively. The mean fiber position itself does not explain the longitudinal arrangement of a fiber or its migratory behavior, as it merely represents its average radial position with respect to the yarn central axis. However, the standard deviation of the mean fiber position for both yarns H and L was quite high compared to the average value of the mean position of all fibers inside the respective yarns. This indicates the variation in mean position of various fibers inside the yarn, as some of them were located at higher radial distances from the yarn center, while others were located quite close to the yarn center.

The mean amplitudes of fiber migration for yarns H and L were 0.43 and 0.36, respectively. The higher value of amplitude of migration refers to the higher amount of deviation of a fiber from its mean position, which also indicates a higher extent of fiber migration taking place inside the yarn. The amplitude of migration had a higher value for yarn H compared to yarn L. However, this difference was not statistically significant. One reason for the lack of significant difference between the amplitude of migration was that each individual fiber (depending on their position within the yarn cross-section) exhibited different migratory behavior. Some fibers showed a higher amplitude of fiber migration under the influence of residual spinning stress, while other fibers showed less amplitude of fiber migration as they were not equally stressed. When the amplitude of fiber migration was averaged, the differences between the two yarns become non-significant (P-value = 0.11) due to the higher values of the standard deviation. The mean migration intensities for yarns H and L were 1.61 and 1.36, respectively, indicating that the average slope of fiber trajectories in yarn H was higher than in yarn L. The difference in the fiber migration intensities was also statistically significant (P-value = 0.001). The higher value for mean migration intensity in yarn H indicated more frequent radial displacement of fibers, which refers to a higher extent and frequency of fiber migration inside the yarn. Similarly, the migration factor (which is a product of migration intensity and the migration amplitude) was higher for yarn H (i.e. 0.23) than yarn L (i.e. 0.16).

The parameters related to longitudinal arrangement of fibers also agreed closely with the previous studies, where these measurements were conducted using the tracer fiber technique.[6,7,11] It was noted that superior quality yarns also exhibited a higher extent of fiber migration. For example, the migration parameters were on the higher side for compact yarns compared to regular ring yarns. Similarly, higher strength was observed for low torque yarns, where the extent for fiber migration was also higher compared to regular ring yarns.[7]

The comparison of the effects of fiber arrangement within the yarn cross-section and along the yarn length on its tensile strength suggests that the fiber arrangement along the yarn length significantly affects the yarn strength. The overall higher values of the parameters related to the longitudinal arrangement of fibers within a yarn represent a higher extent of fiber migration occurring inside yarn H. The frequent and broader radial disposition of fibers together could produce a more integrated yarn structure, as fibers would be more 'intertwined' together. This could be assumed to provide improved cohesion to the yarn, allowing it to withstand comparatively higher tensile stresses.

Conclusions

This study examined the use of micro CT scanning along with digital image processing as a method to comprehensively study and compare the arrangement of fibers within a yarn. Micro CT scanning is both a non-invasive and comprehensive analysis technique, which provides complete information about the internal yarn structure and overcomes the limitations associated with the existing methods. However, a notable concern associated with high-resolution CT scanning is the undesired compromise on the field of view of the CT system, which also significantly reduces the scannable yarn length.

It was found that helical type micro CT scanning was a more suitable approach compared to regular CT scanning due to its ability to scan specimens with high aspect ratios. The proposed digital image processing algorithms when applied on the micro CT dataset achieved through helical CT method effectively analyzed the fiber arrangement inside the yarns. Hence, this combined method could be applied on a variety of yarn specimens to achieve a deeper and comprehensive understanding of the internal yarn structure and to establish its effect on the resultant yarn properties.

This work also showed that the longitudinal arrangement of fibers in terms of their migratory behavior had a decisive influence on the tensile

properties of the yarn. The stronger yarn showed a higher value of the amplitude and intensity of fiber migration compared to the weaker yarn, which referred to a more cohesive yarn structure due to higher extent of fiber migration. However, this observation was based only on two yarn specimens; utilizing the proposed method to study wider yarn samples will allow a better understanding of these relationships.

Acknowledgement

The authors would like to acknowledge the technical support provided by Dr Levi Beeching (Australian National University) and Dr Asadul Haque (Monash University) in the micro CT scanning of yarn specimens.

Declaration of conflicting interests

The authors declared no potential conflicts of interest with respect to the research, authorship, and/or publication of this article.

Funding

The authors received no financial support for the research, authorship, and/or publication of this article.

ORCID iD

Xungai Wang http://orcid.org/0000-0002-3549-6769

References

1. Morton WE. The arrangement of fibers in single yarns. *Text Res J* 1956; 26: 325–331.
2. Schwarz ER. Certain aspects of yarn structure. *Text Res J* 1951; 21: 125–136.
3. Yilmaz D, Göktepe F, Göktepe Ö, et al. Packing density of compact yarns. *Text Res J* 2007; 77: 661–667.
4. Hussain U, Shafqat A, Iqbal M, et al. Effect of spinning variables on packing density of cotton yarn. *Ind J Fibre Text Res* 2014; 39: 434–436.
5. Jiang XY, Hu JL, Cheng KPS, et al. Determining the cross-sectional packing density of rotor spun yarns. *Text Res J* 2005; 75: 233–239.
6. Basal G and Oxenham W. Comparison of properties and structures of compact and conventional spun yarns. *Text Res J* 2006; 76: 567–575.
7. Guo Y, Tao X, Xu B, et al. Structural characteristics of low torque and ring spun yarns. *Text Res J* 2011; 81: 778–790.
8. Neckář B, Ishtiaque S and Švehlová L. Rotor yarn structure by cross-sectional microtomy. *Text Res J* 1988; 58: 625–632.
9. Chollakup R, Osselin J-F, Sinoimeri A, et al. Effects of blending parameters on the cross-section fiber migration of silk/cotton Blends. *Text Res J* 2008; 78: 361–369.
10. Riding G. Filament migration in single yarns. *J Text Inst Trans* 1964; 55: T9–T17.
11. Huh Y, Kim YR and Ryu WY. Three-dimensional analysis of migration and staple yarn structure. *Text Res J* 2001; 71: 81–90.
12. Eldessouki M and Ibrahim S. Chan-Vese segmentation model for faster and accurate evaluation of yarn packing density. *Text Res J* 2015; 86: 167–177.
13. Li SY, Xu BG, Tao XM, et al. An intelligent computer method for automatic mosaic and segmentation of tracer fiber images for yarn structure analysis. *Text Res J* 2015; 85: 733–750.
14. Primentas A and Iype C. The configuration of textile fibres in staple yarns. *J Text Apparel Technol Manag* 2001; 1: 1–8.
15. Chiu SH and Liaw JJ. Fiber recognition of pet/rayon composite yarn cross-sections using voting techniques. *Text Res J* 2005; 75: 442–448.
16. Lawrence CA. *Advances in yarn spinning technology*. Cambridge: Woodhead Publishing Limited, 2010, p.223.
17. Toda M and Grabowska KE. Computed microtomography in the analysis of fiber migration in yarn. *Autex Res J* 2013; 13: 28–32.
18. Toda M, Grabowska KE and Ciesielska-Wrobel IL. Micro-CT supporting structural analysis and modelling of ropes made of natural fibers. *Text Res J* 2015; 86: 1280–1293.
19. Yamasaki E, Sakurada S, Nakamura R, et al. Identification of migration structure in a natural fiber twisted yarn and its effect on tensile strength. *J Soc Mater Sci Jpn* 2015; 64: 215–222.
20. Toda M, Grabowska K and Ciesielska-Wróbel I. Application of micro-computed tomography (micro-CT) to study unevenness of the structure of yarns. *Text Res J* 2017; 87: 351–368.
21. Haleem N. *Dynamics of spinning triangle geometry and its effects on yarn quality*. PhD Thesis, Deakin University, Australia, 2017.
22. Wang X and Chang L. Reducing yarn hairiness with a modified yarn path in worsted ring spinning. *Text Res J* 2003; 73: 327–332.
23. Wei L, Huang S, Zhu T, et al. Research on shape of spinning triangles in the ring spinning system. *J Text Inst* 2016; 107: 420–430.
24. Singh C, Gordon S and Wang X. The mechanism of hairiness reduction in offset ring spinning with a diagonal yarn path. *Text Res J*. (May 10, 2018): 004051751877591. doi:10.1177/0040517518775915.
25. Otsu N. A threshold selection method from gray-level histograms. *Automatica* 1975; 11: 23–27.
26. Majumdar A. *Principles of woven fabric manufacturing*. Florida: CRC Press, 2016, p.33.
27. Gonzalez RC and Woods RE. *Digital image processing*. London: Pearson Education, 2011, pp.694–695.
28. Merkus HG. *Particle size measurements: Fundamentals, practice, quality*. Dordrecht: Springer Netherlands, 2009, p.17.

29. Heilbronner R and Barrett S. *Image analysis in earth sciences: Microstructures and textures of earth materials*. Berlin, Heidelberg: Springer, 2013, pp.320–328.
30. Hearle JWS, Gupta BS and Merchant VB. Migration of fibers in yarns: Part I: Characterization and idealization of migration behavior. *Text Res J* 1965; 35: 329–334.
31. Slater K. Yarn evenness. *Text Progr* 1986; 14: 1–90.
32. Zou Z, Zheng S, Cheng L, et al. Effect of some variables on the fibre packing pattern in a yarn cross-section for vortex spun yarn. *Fibre Text East Eur* 2014; 22: 40–46.
33. Ishtiaque SM, Mukhopadhyay A and Kumar A. Impact of high-speed draw frame and its preparatory on packing and related characteristics of ring spun yarn. *J Text Inst* 2009; 100: 657–667.
34. Ishtiaque S, Subramani P, Kumar A, et al. Structural and tensile properties of ring and compact plied yarns. *Ind J Fibre Text Res* 2009; 34: 213–238.